Materials Technology Reports 2024, 2(2), 1699.
https://doi.org/10.59400/mtr1699

Article

Preparation and characterization of $CuBO_2$-based photocatalysts and doped variants

Soheila Azordeh[1,*], Mehdi Asadi[2], Abdolali Alemi[1,*]

[1] Department of Chemistry, Tabriz University, Tabriz 5166616471, Iran
[2] Faculty of Natural Sciences, Geochemistry and Gemological Laboratory, University of Tabriz, 5166616471 Tabriz, Iran
*** Corresponding authors:** Soheila Azordeh, soheila.azorde@gmail.com; Abdolali Alemi, alemi@tabrizu.ac.ir

CITATION

Azordeh S, Asadi M, Alemi A. Preparation and characterization of $CuBO_2$-based photocatalysts and doped variants. Materials Technology Reports. 2024; 2(2): 1699. https://doi.org/10.59400/mtr1699

ARTICLE INFO

Received: 6 September 2024
Accepted: 20 November 2024
Available online: 26 November 2024

Abstract: An eco-friendly $CuBO_2$-based photocatalyst has been doped by a lanthanide for the first time. Gd^{3+} and Gd^{3+}/Bi^{3+}-doped $CuBO_2$ are synthesized by the hydrothermal method to study their magnetic properties. Then they are analyzed by XRD, UV-Vis, SEM, and VSM. The maximum amount of doping is x= 0 − 1.5% in $Cu_{1-3x}Gd_{3x}BO_2$ and $Cu_{1-3x}Bi_{3x/2}Gd_{3x/2}BO_2$ formulas as they are analyzed in XRD. For concentrations higher than x = 2%, the additional peak indicates that doping is incomplete. The XRD pattern of CuBO2 confirms that its crystal structure is a hexagonal one with the $R\bar{3}m$ space group. According to UV-Vis analysis, the bandgap energies are 2.711, 2.753, and 2.765 for $CuBO_2$ and doped systems. Additionally, the morphology of particle sizes is confirmed according to SEM images. Meanwhile, the magnetic properties of synthesized material are studied by VSM, and the doped compound exhibited higher magnetic properties than $CuBO_2$, which is associated with the exchange interaction of electron and d spins in Gd^{3+} and Bi^{3+}. The study aims to provide insights into the magnetic properties of lanthanide-doped $CuBO_2$-based photocatalysts, potentially paving the way for developing improved magnetic materials for various applications.

Keywords: bandgap energy; $CuBO_2$; photocatalyst; lanthanide; magnetic properties

1. Introduction

One of the most intriguing issues for materializing oxide-based electronics is researching and expanding p-type wide-bandgap oxide materials. In order to achieve technologies such as electronics that are invisible and utilize wide bandgaps, p-type transparent conducting oxides (TCOs) are considered as key factors due to their appropriate electrical and optical features [1].

In the last decades, $CuBO_2$ has been known as the newest material among Copper delafossites, which can be as a hopeful electrical conductivity and splendid transparency at room temperature. However, few studies have been conducted on this important and valuable material [2–4]. This material with high photocatalytic activity was introduced as a p-type material of the environment-friendly TCO group by Chattopadhyay's research group [1].

Copper metaborate belongs to the group of oxide copper compounds and has various magnetic features [5]. Hence, Roessli et al. have reported that temperature changes affect the magnetic phase of such material and the phase changes from the paramagnetic to the commensurate weak ferromagnetic by decreasing temperature at $10 \leq T \leq 21$ K under zero magnetic field [6].

There are other various types of these compounds, i.e., CuB_2O_4, $Cu_3B_2O_6$, $Cu_2[BO(OH)_2](OH)_3$, $Cu_3B_6O_{12}{\cdot}H_2O$ and $Cu_3B_6O_{12}$ each of which is utilized in the

optical devices and electrodes according to their magnetic and electrical properties, respectively [7].

Chattopadhyay et al. studied the photocatalytic performance of this delafossite material for the first time with a standard photocatalytic set-up that showed the photocatalytic efficiency increased with decreasing particle size. The efficient photocatalytic performance made this novel p-type wide bandgap semiconductor an indeed multifunctional material [1].

In another study, Mero et al. studied the optical features of copper metaborate by spectroscopic ellipsometry and Raman scattering spectroscopy. The results illustrated that temperature reduction caused an unusual redshift to appear in the bandgap. In addition, upon cooling at 21 K—that is, the canted antiferromagnetic ordering temperature—the irregularities were observed in the bandgap, peak energy, and normalized intensity of charge transfer bands [8].

Scanlon et al. have utilized GGA corrected for on-site Coulomb interactions (GGA + U) and a hybrid density functional (HSE06) for investigating and computing the geometry and electronic structure of $CuBO_2$. The analysis of band extrema shows that boron (B) does not contribute to the state that controls conductivity. Also, good p-type conductivity was forecast. It is noticeable that the smaller Cu-Cu distance in such material in comparison with any other delafossites caused this increasing conductivity [4].

Other studies have investigated changes in the magnetic and optical properties of doped copper metaborate by Ni^{2+} and Mn^{2+} [9–11]. Doping is a common method used to intentionally introduce impurities (other cations) into the structure of semiconductors, thereby changing their electrical, optical, and magnetic properties, and improving their bandgap properties [12–14]. Hence, Khanh et al. demonstrated that electric polarization can be created and controlled in doped copper metaborate by Ni^{2+} under a magnetic field by investigating the magnetoelectric effect in the Ni/copper metaborate system [9].

On the other hand, lanthanides have recently gained attention due to their magnetic, optical, and electrical properties [15–19].

In this study, gadolinium has been selected as a lanthanide with magnetic properties [20,21], and the changes in the magnetic properties of doped copper metaborate by Gd^{3+} and Gd^{3+}/Bi^{3+} are compared. Notably, this is the first time a lanthanide has been doped into the copper metaborate structure in order to improve its magnetic properties.

2. Materials and methods

Copper acetate (99.99%), borax (99.0%), and bismuth nitrate pentahydrate (99.99%) purchased from Sigma-Aldrich, and sodium hydroxide (99.0%) and gadolinium oxide (99.9%) purchased from Merck, were used in the synthesis method. The purity of used materials is 99%. Also, XRD (Siemens D500), SEM (TESCAN MIRA3-FEG), UV-Vis (Sinco 4100), and VSM 7400 Lake Shore (VSM) are used for analyzing synthesized nanostructures.

2.1. Synthesis of $Cu_{1-3x}Gd_{3x}BO_2$

Gadolinium oxide was dissolved in the minimum amount of nitric acid according to **Table 1** with a determined molar ratio to use its nitrate in the reaction. Then copper acetate and 0.04 molar borax solutions are prepared in a separate beaker and added into the gadolinium-nitrate solution, and stirred for 30 min at 25 ℃. Next, 0.2 molars of NaOH are added to the main solution and stirred for 2 min at the same temperature. The mixture will be entered into the autoclave and heated for 10 hours at 180 ℃. The last step is cooling, filtering, washing with deionized water, and drying the obtained powder at room temperature [1,22,23].

Table 1. The ratio of used materials for the synthesis of $Cu_{1-3x}Gd_{3x}BO_2$.

Sample	Nitric acid (M)	Borax (mol)	Gadolinium oxide (mol)	Copper acetate (mol)	*x* (%)
A	0.2	0.0008	0.0062	0.003341	0.005
B			0.0124	0.003324	0.01
C			0.0186	0.003307	0.015
D			0.0248	0.003290	0.02

2.2. Synthesis of $Cu_{1-3x}Gd_{3x/2}Bi_{3x/2}BO_2$

Gd^{3+}/Bi^{3+} doped-$CuBO_2$ catalyst was synthesized by the same method in 2.1. The difference is that the ratio of used materials is according to **Table 2**.

Table 2. The ratio of used materials for the synthesis of $Cu_{1-3x}Gd_{3x/2}Bi_{3x/2}BO_2$.

Sample	Nitric acid (M)	Borax (mol)	Bismuth nitrate (mol)	Gadolinium oxide (mol)	Copper acetate (mol)	*x* (%)
A	0.2	0.0008	0.000017	0.0062	0.003324	0.01
B			0.0000255	0.0093	0.003307	0.015
C			0.000034	0.0124	0.003290	0.02

3. Results and discussion

3.1. XRD Pattern

According to the JCPDS card (No. 28–1256), the synthesized $CuBO_2$ organizes a hexagonal structure with an $R3\bar{m}$ space group [24,25]. XRD patterns in **Figure 1a,b,c** show there is no additional peak to behold in x = 1.5%. It can be concluded that Gd^{3+} is solvable in the $Cu_{1-3x}Gd_{3x}BO_2$ system up to x = 1.5%, while when x goes to 2%, there will be three additional peaks at 2θ = 28.15, 36.45, and 52.22. This could be related to oxidized non-doped gadolinium in the process of synthesis. **Figure 1d** indicates that incomplete doping is in accordance with gadolinium oxide peaks in the JCPDS card (No. 42–1465).

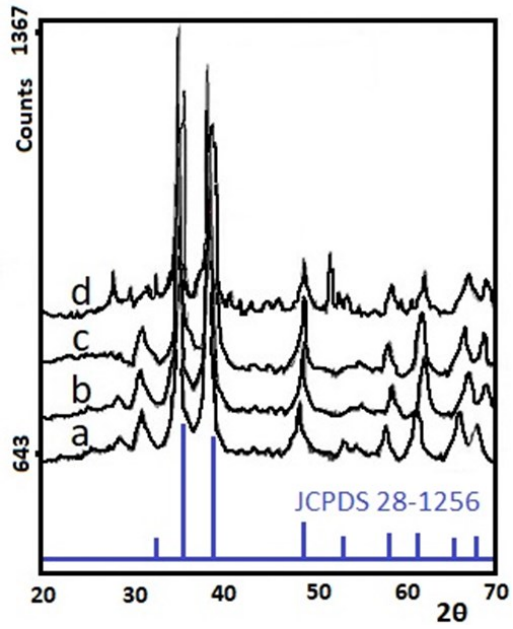

Figure 1. XRD patterns of $Cu_{1-3x}Gd_{3x}BO_2$ (**a**) x = 0.5%; (**b**) x = 1%; (**c**) x = 1.5%; and (**d**) x = 2%.

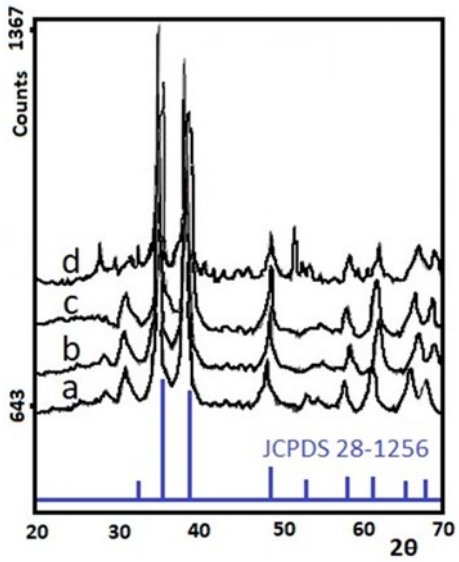

Figure 2. XRD spectra of (**a**) $Cu_{1-3x}Gd_{3x/2}Bi_{3x/2}BO_2$ (x = 1%); (**b**) $Cu_{1-3x}Gd_{3x/2}Bi_{3x/2}BO_2$ (x = 1.5%); (**c**) $Cu_{1-3x}Gd_{3x/2}Bi_{3x/2}BO_2$ (x = 2%).

Based on XRD spectra in **Figures 2a,b**, it can be concluded that Bi^{3+} and Gd^{3+} are soluble in $Cu_{1-3x}Gd_{3x/2}Bi_{3x/2}BO_2$ system at the same concentration (x = 1.5%). **Figure 2c** illustrates that when x increases to 2%, there will be an additional peak at 2θ = 42.89, which shows incomplete doping.

3.2. UV-Vis analysis

The purpose of carrying out UV-Vis analysis is to calculate the bandgap and investigate electron transfer. **Figure 3** illustrates the UV-Vis spectra of $CuBO_2$, showing that absorption intensity has been increased by doping and a small shift has been observed in the wavelengths.

Indeed, electron transfer in copper metaborate is related to ligand-to-metal charge transfer [LMCT]. The absorption band is near 457 nm. This could be related to the electron transfer from the oxygen 2p orbital to the copper 4s orbital [LMCT].

It should be mentioned that LMCT is electron transfer from the valence band (O^{2-} : 2*p*) to the conductive band (Cu^{+}: 4*s*). There is no d-to-d orbital electron transfer because d orbitals are occupied in Cu^{+}. This applies to Bi^{3+} (6*p*) too. But f orbitals (4*f*) are partially filled in Gd^{3+}; therefore, *f*-to-*f* orbital electron transfer can occur. Hence, they have shifted to shorter wavelengths.

In order to calculate bandgap energy, Equation (1) is used, where h is Planck's constant, c is the velocity of light, and λ is the wavelength [26]:

$$E = hc/\lambda$$
$$E = 1239/\lambda \text{ (eV)} \quad (1)$$

The calculated bandgap energies for $CuBO_2$, $Cu_{1-3x}Gd_{3x}BO_2$, and $Cu_{1-3x}Gd_{3x/2}Bi_{3x/2}BO_2$ are 2.711, 2.753, and 2.765 eV, respectively.

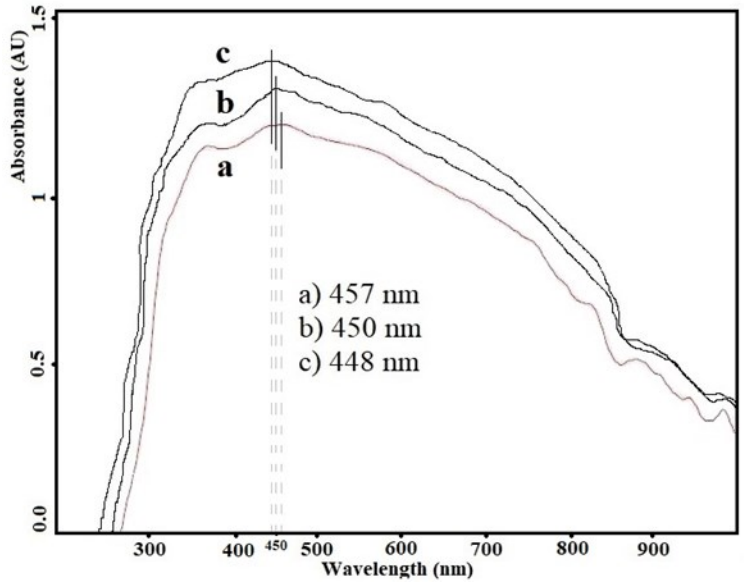

Figure 3. UV-Vis spectra of (**a**) $CuBO_2$ nanopowders; (**b**) $Cu_{1-3x}Gd_{3x}BO_2$ (x = 1.5%); and (**c**) $Cu_{1-3x}Gd_{3x/2}Bi_{3x/2}BO_2$ (x = 1.5%).

3.3. Magnetic spectra analysis

Magnetic measurements of samples were performed by VSM. The results are demonstrated in the magnetization curves based on magnetic field strength. **Figure 4a–c** indicates magnetization curves based on the magnetic field in synthesized nanopowders for different x at room temperature. As seen, all samples include a hysteresis curve, so they have paramagnetic properties. (Hc) and (Ms) of samples are seen in graphs.

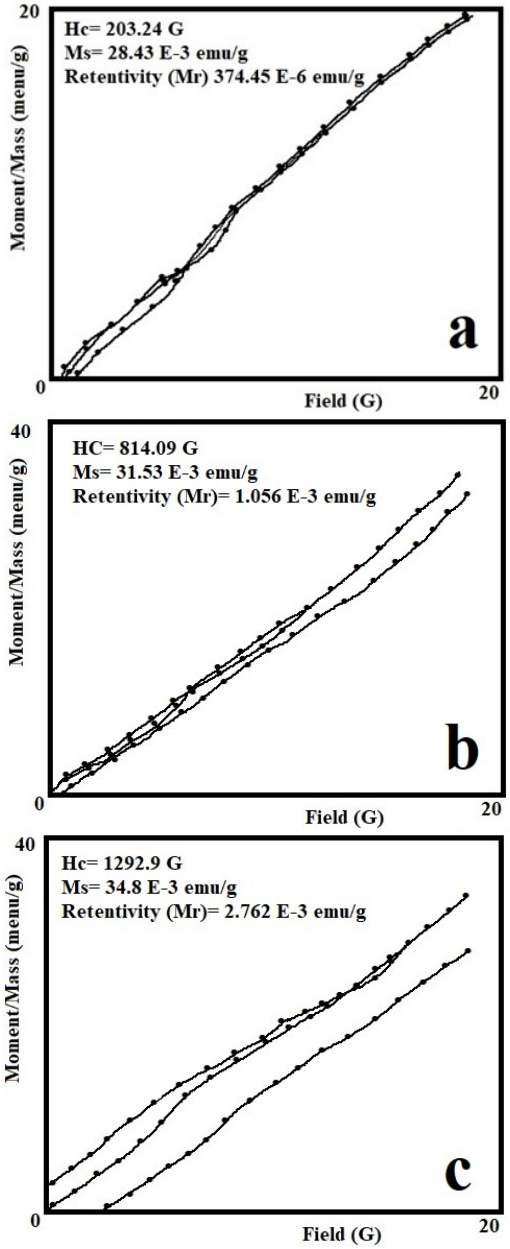

Figure 4. Magnetization curve on the basis of the external magnetic field in room temperature of **(a)** $CuBO_2$ nanopowders; **(b)** $Cu_{1-3x}Gd_xBO_2$ (x = 1.5%); and **(c)** $Cu_{1-3x}Gd_{3x/2}Bi_{3x/2}BO_2$ (x = 1.5%).

As can be seen in **Figure 4**, (Ms) increases as the type of doped element changes. This is because of the increase in the replacement magnetic moment in the host network [27]. Indeed, in a magnetic network, electrons will be polarized by the injection of magnetic ions at a determined level. It is the result of exchange interactions in Ruderman-Kittel-Kasuya-Yosida (RKKY). This impurity can have paramagnetic properties [28]. Therefore, paramagnetic features in doped compositions are obtained by the exchange interaction of electron and d spins in Gd^{3+} and Bi^{3+}. The interaction can cause a regular arrangement of adjacent spins and the magnetization of the network.

3.4. SEM images

The purpose of electron microscopy images is the analysis of surface morphology, grain size, and distribution. The magnifications of 30000x and 50000x for analyzing powders were used (**Figure 5**). The frequency of particles shows that their size is around 60 nm. It should be mentioned that the distribution is high and the highest frequency is in the range of 59 nm to 65 nm.

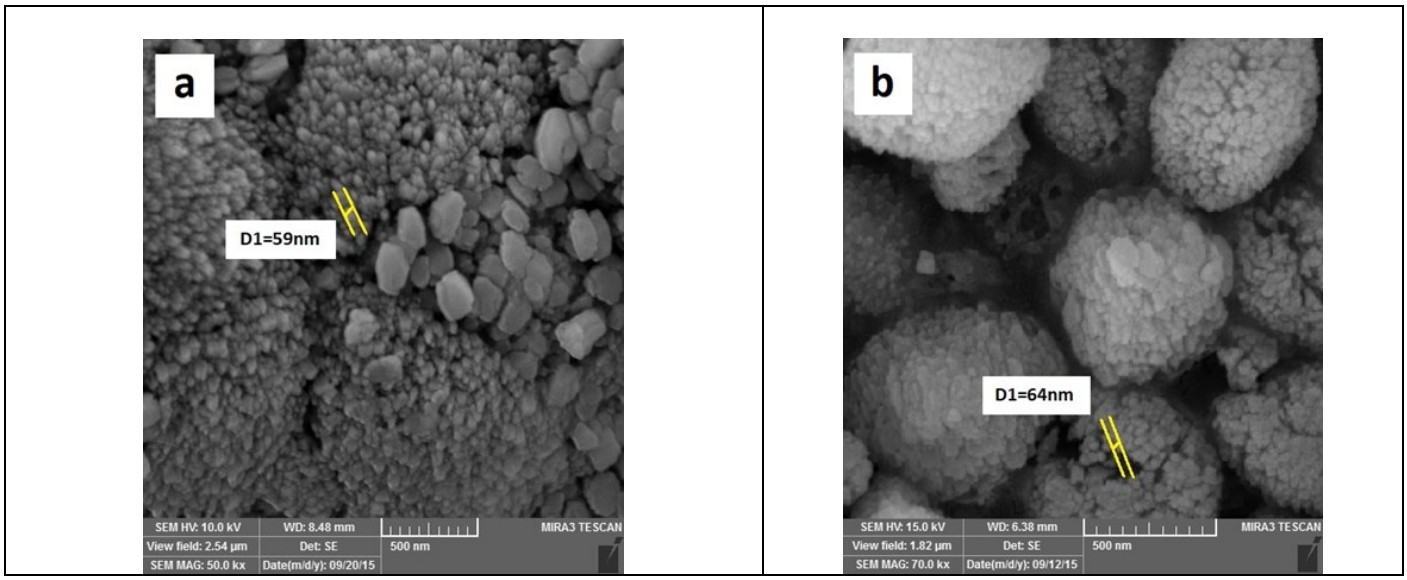

Figure 5. SEM image of **(a)** $Cu_{1-3x}Gd_{3x}BO_2$; and **(b)** $Cu_{1-3x}Gd_{3x/2}Bi_{3x/2}BO_2$.

4. Conclusion

This study successfully doped nano $CuBO_2$ with a lanthanide for the first time. The XRD pattern of the synthesized samples illustrated that the maximum amount of doping is $x = 0 - 1.5\%$. In concentrations higher than $x = 2\%$, additional peaks are observed that indicate doping is incomplete. LMCT is electron transfer from the valence band (O^{2-}: 2*p*) to the conductive band (Cu^{+}: *4s*). There is no *d*-to-*d* orbital electron transfer because *d* orbitals are occupied in Cu^{+}. This applies to Bi^{3+} (6*p*) too. But *f* orbitals (4*f*) are partially filled in Gd^{3+}, so *f*-to-*f* orbital electron transfer can be carried out. Hence, they have shifted to shorter wavelengths, and the calculated bandgap energies for $CuBO_2$, $Cu_{1-3x}Gd_{3x}BO_2$, and $Cu_{1-3x}Gd_{3x/2}Bi_{3x/2}BO_2$ are 2.711, 2.753, and 2.765 *eV*, respectively. Magnetic curves of samples demonstrated that all of the samples include hysteresis curves, and (Ms) increases as the type of doped element changes. It is because of the increase in the replacement magnetic moment in the host network. Therefore, paramagnetic properties in doped compositions are obtained by the exchange interaction of electron and *d* spins in Gd^{3+} and Bi^{3+}. The interaction can cause a regular arrangement of adjacent spins and the magnetization of the network.

Author contributions: Conceptualization, SA and MA; methodology, SA; software, SA; validation, SA and AA; formal analysis, SA and AA; investigation, SA and MA; resources, SA and MA; data curation, SA and AA; writing—original draft preparation, SA and MA; writing—review and editing, SA and MA; visualization,

SA; supervision, AA; project administration, SA and AA; funding acquisition, AA. All authors have read and agreed to the published version of the manuscript.

Conflict of interest: The authors declare no conflict of interest.

References

1. Santra S, Das NS, Chattopadhyay KK. Wide band gap p-type nanocrystalline CuBO2 as a novel UV photocatalyst. Materials Research Bulletin. 2013; 48(7): 2669–2677. doi: 10.1016/j.materresbull.2013.03.034
2. Snure M, Tiwari A. CuBO2: A p-type transparent oxide. Applied Physics Letters. 2007; 91(9). doi: 10.1063/1.2778755
3. Zheng Y, Wang Z, Tian Y, et al. Synthesis and performance of 1D and 2D copper borate nano/microstructures with different morphologies. Colloids and Surfaces A: Physicochemical and Engineering Aspects. 2009; 349(1–3): 156–161. doi: 10.1016/j.colsurfa.2009.08.012
4. Scanlon DO, Walsh A, Watson GW. Understanding the p-Type Conduction Properties of the Transparent Conducting Oxide CuBO2: A Density Functional Theory Analysis. Chemistry of Materials. 2009; 21(19): 4568–4576. doi: 10.1021/cm9015113
5. Bolsunovskaya O, Popov M, Petrakovskii G, et al. Magnetic structure and elementary excitation spectra of copper metaborate. Journal of Magnetism and Magnetic Materials. 2006; 300(1): e392–e394. doi: 10.1016/j.jmmm.2005.10.127
6. Roessli B, Schefer J, Petrakovskii GA, et al. Formation of a Magnetic Soliton Lattice in Copper Metaborate. Physical Review Letters. 2001; 86(9): 1885–1888. doi: 10.1103/physrevlett.86.1885
7. Kipcak AS, Senberber FT, Aydin Yuksel S, et al. Synthesis, characterisation, electrical and optical properties of copper borate compounds. Materials Research Bulletin. 2015; 70: 442–448. doi: 10.1016/j.materresbull.2015.05.003
8. Mero RD, Lai CH, Du CH, et al. Spectroscopic Signature of Spin–Charge–Lattice Coupling in CuB2O4. The Journal of Physical Chemistry C. 2021; 125(7): 4322–4329. doi: 10.1021/acs.jpcc.1c00111
9. Khanh ND, Abe N, Kubo K, et al. Magnetic control of electric polarization in the noncentrosymmetric compound (Cu,Ni)B2O4. Physical Review B. 2013; 87(18). doi: 10.1103/physrevb.87.184416
10. Molchanova AD, Boldyrev KN, Erofeev AS, et al. Magnetic phase transitions and linear magnetic dichroism in manganese-doped copper metaborate (Cu,Mn)B2O4. Journal of Physics: Conference Series. 2017; 917: 072003. doi: 10.1088/1742-6596/917/7/072003
11. A.D. Molchanova, E.M. Moshkina, M.S. Molokeev, E.V. Tropina, A.F. Bovina, K.N. Boldyrev, Synthesis and optical properties of nickel-doped copper metaborate crystals, Opt. Spectrosc. 2022, 130.
12. Giri S, Trewyn BG, Stellmaker MP, et al. Stimuli—Responsive Controlled—Release Delivery System Based on Mesoporous Silica Nanorods Capped with Magnetic Nanoparticles. Angewandte Chemie International Edition. 2005; 44(32): 5038–5044. doi: 10.1002/anie.200501819
13. Bergemann C, Muller-Schulte D, Oster J, et al. Magnetic ion-exchange nano- and microparticles for medical, biochemical and molecular biological applications. J. Magn. Magn. Mater. 1999; 194: 45.
14. Nunez L, Kaminski MD. Transuranic separation using organophosphorus extractants adsorbed onto superparamagnetic carriers. J. Magn. Magn. Mater. 1999; 194: 102.
15. Ellis MC. Understanding Magnetic and Optical Properties of Lanthanide-Doped Oxide Nanospinels and Heterometallic Formate Metal-Organic Frameworks [PhD thesis]. Florida State University Libraries; 2020.
16. Reisfeld R. Optical Properties of Lanthanides in Condensed Phase, Theory and Applications. AIMS Materials Science. 2015; 2(2): 37–60. doi: 10.3934/matersci.2015.2.37
17. Brik MG, Srivastava AM. 1.8 Electronic properties of the lanthanide ions. Rare Earth Chemistry. 2020: 83–96. doi: 10.1515/9783110654929-008
18. Kurzen H, Bovigny L, Bulloni C, et al. Electronic structure and magnetic properties of lanthanide 3+ cations. Chemical Physics Letters. 2013; 574: 129–132. doi: 10.1016/j.cplett.2013.04.070
19. Sorace L, Gatteschi D. Lanthanides and an Actinides in molecular magnetism 1st ed. In:Electronic Structure and Magnetic Properties of Lanthanide Molecular Complexes. Wiley-VCH Verlag GmbH & Co. KGaA; 2015.
20. Ncube S, Coleman C, Strydom A, et al. Kondo effect and enhanced magnetic properties in gadolinium functionalized carbon nanotube supramolecular complex. Scientific Reports. 2018; 8(1). doi: 10.1038/s41598-018-26428-y
21. Serga V, Burve R, Maiorov M, et al. Impact of Gadolinium on the Structure and Magnetic Properties of Nanocrystalline Powders of Iron Oxides Produced by the Extraction-Pyrolytic Method. Materials. 2020; 13(18): 4147. doi:

10.3390/ma13184147

22. Bae J, Shin D, Jeong H, et al. Highly Water-Resistant La-Doped Co3O4 Catalyst for CO Oxidation. ACS Catalysis. 2019; 9(11): 10093–10100. doi: 10.1021/acscatal.9b02920
23. Santra S, Das NS, Maiti S, et al. Wide band gap p-type CuBO2 nanostructures by hydrothermal route and fabrication high quality p-CuBO2/n-ZnO nano-heterojunction. Chemical Physics Letters. 2014; 604: 97–100. doi: 10.1016/j.cplett.2014.04.052
24. Ruttanapun C. Optical and electronic properties of delafossite CuBO2 p-type transparent conducting oxide. Journal of Applied Physics. 2013; 114(11): 113108. doi: 10.1063/1.4821960
25. Santra S, Das NS, Chattopadhyay KK. Sol–gel synthesis and characterization of wide band gap p-type nanocrystalline CuBO2. Materials Letters. 2013; 92: 198–201. doi: 10.1016/j.matlet.2012.10.094
26. Connors KA. The Phenomenological Theory of Solvent Effects in Mixed Solvent Systems. Handbook of Solvents. 2014: 467–490. doi: 10.1016/b978-1-895198-64-5.50013-1
27. Madhusudan KR, Manorama SV, Ramachandra RA. Bandgap studies on anatase titanium dioxide nanoparticles. Mater. Chem. Phys. 2003; 78: 239.
28. Morales AE, Mora ES, Pal U. Use of diffuse reflectance spectroscopy for optical characterization of un-supported nanostructures. Rev. Mex. de Fis. 2007; 53: 18.